Chemical Research in Toxicology

Article

pubs.acs.org/crt

Contrast of the Biological Activity of Negatively and Positively Charged Microwave Synthesized CdSe/ZnS Quantum Dots

Amber Nagy,[†] Andrew Zane,[‡] Sara L. Cole,[§] Michael Severance,[‡] Prabir K. Dutta,*[,‡] and W. James Waldman*[,†]

[†]Department of Pathology, The Ohio State University, Columbus, Ohio, United States

[‡]Department of Chemistry, The Ohio State University, Columbus, Ohio, United States

[§]Campus Microscopy and Imaging Facility, The Ohio State University, Columbus, Ohio, United States

Supporting Information

ABSTRACT: Quantum dots (QDs) are semiconductor nanocrystals that have found use in bioimaging, cell tracking, and drug delivery. This article compares the cytotoxicity and cellular interactions of positively and negatively charged CdSe/CdS/ZnS QDs prepared by a microwave method using a murine alveolar macrophage-like cell culture model. Keeping the core semiconductor the same, QD charge was varied by altering the surface capping molecule; negatively charged QDs were formed with mercaptopropionic acid (MPA-QDs) and positively charged QDs with thiocholine (THIO-QDs). The size and charge of these two QDs were investigated in three types of media (RPMI, RPMI + FBS, and X-VIVO serum-free media) relevant for the biological studies. MPA-QDs were found to have negative zeta potential in RPMI, RPMI + FBS, and serum-free media and had sizes ranging from 8 to 54 nm. THIO-QDs suspended in RPMI alone were <62 nm in size, while large aggregates (greater than 1000 nm) formed when these QDs were suspended in RPMI + FBS and serum-free media. THIO-QDs retained positive zeta potential in RPMI and were found to have a negative zeta potential in RPMI + FBS and nearly neutral zeta potential in serum-free media. In a cell culture model, both MPA-QDs and THIO-QDs caused comparable levels of apoptosis and necrosis. Both QDs induced significant tumor necrosis factor-alpha (TNF-α) secretion only at high concentrations (>250 nM). Both types of QDs were internalized via clathrin-dependent endocytosis. Using real-time, live cell imaging, we found that MPA-QDs interact with the cell surface within minutes and progress through the endocytic pathway to the lysosomes upon internalization. With the THIO-QDs, the internalization process was slower, but the pathways could not be mapped because of spectroscopic interference caused by QD aggregates. Finally, MPA-QDs were found to associate with cell surface scavenger receptors, while the THIO-QDs did not. This study indicates that the surface charge and aggregation characteristics of QDs change drastically in biological culture conditions and, in turn, influence nanoparticle and cellular interactions.

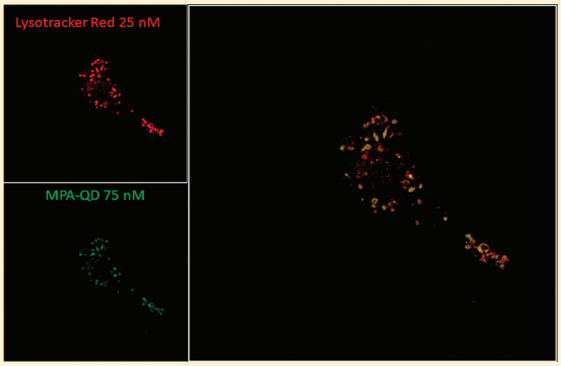

INTRODUCTION

The emergence of nanotechnology has ushered in many new and exciting applications. The use of nanoparticles in biomedicine has already proved to be quite useful as demonstrated by the increase of FDA-approved treatments that have incorporated the use of nanosized drug carriers. Quantum dots (QDs) are fluorescent semiconductor nanoparticles that have several advantages over traditional organic fluorophores. Because they are resistant to photobleaching, size tunable, and have the ability to be multiplexed, they are already being used in both clinical and basic sciences as tools for microbial detection,[1−4] bioimaging,[5−7] drug delivery,[8−10] and tracking.[11−14] One of the most interesting and effective applications of QDs is their use in imaging. Because of their size and robust fluorescence, they can be used in single molecule tracking.[11,12,14−16] Cancer cell lines were among the first live cells that were successfully imaged,[6,17] and QDs have been used to visualize receptor interactions, specifically erb2/HER receptor mediated signal transduction[18] and neuronal glycine receptors.[12]

Studies have been conducted that investigate the cytotoxicity of QDs with particular focus on QDs with Cd cores. One early study showed that differences in CdSe QD toxicity in Vero cells, HeLa cells, and human primary hepatocytes were concentration and time dependent.[19] Size dependent cytotoxicity in rat pheochromocytoma cells and murine microglial cells was confirmed by Lovrić et al.[20] using CdTe QDs. The mechanism of QD cytotoxicity in MCF-7 breast cancer cells has been attributed to the formation of reactive oxygen species (ROS).[21] Others[22] showed that QD internalization by hippocampal neurons resulted in calcium deregulation and sodium channel disruption, both of which can affect the role of ROS mediated protective responses.

Received: August 2, 2011
Published: November 17, 2011

The mechanism by which nontargeted nanoparticles enter cells is not well understood, and there is evidence that multiple pathways may be used. One recent study reported that commercially available negatively charged QDs can use scavenger receptors and lipid raft-mediated endocytosis for cellular entry in epidermal keratinocytes.[23] Modified low density lipids and negatively charged inorganic nanoparticles have the propensity to bind scavenger receptors which supports the role of these receptors in QD uptake. Little research has been conducted regarding the internalization mechanism of positively charged QDs. The intracellular destination of QDs has been shown to range from the cytoplasm and nucleus[24,25] to lysosomes.[23]

Although nanoparticles have shown great promise for use in biomedical applications, there is an urgent need to understand the implications, cellular interactions, and toxicity of nanoparticles harboring different physicochemical properties. In this study, using QDs as a model nanoparticle system, we address this problem by investigating how the physical properties of as-synthesized positive and negative QDs change in biologically relevant media and the influence of these resulting particles on cytotoxicity, inflammation, cellular uptake, and cell surface interactions in an alveolar macrophage cell line. Large quantities of double shelled CdSe/CdS/ZnS QDs were prepared using an inexpensive, rapid, microwave-based protocol, and surface charges were altered by capping QDs with mercaptopropionic acid (MPA-QDs) or thiocholine (THIO-QDs) to produce negative and positively charged QDs, respectively.[26] Because of the ability of nanoparticles in general to traverse the pulmonary system and reach alveoli after intentional or incidental exposure, we chose the murine alveolar macrophage-like cell line, MH-S, for our exposure studies due to their relevance in pulmonary uptake and respiratory toxicology.

A profound difference of the charge and aggregation characteristics of QDs was also revealed in biologically relevant media. MPA-QD and THIO-QD induced cell death, apoptosis, and tumor necrosis factor-alpha (TNF-α) secretion in macrophages after exposure to high concentrations. Both types of QDs appear to utilize clathrin-coated pits for cell entry. The internalization of MPA-QDs was captured in real time, and intracellular fate was found to be confined to lysosomes. Differences in the molecular level interaction of positively and negatively charged QDs with cell surface scavenger receptors are reported for the first time.

EXPERIMENTAL PROCEDURES

Chemicals for QD Synthesis. Cadmium chloride hemipentahydrate, $CdCl_2 \cdot 2.5\ H_2O$ (≥98%), and sodium borohydride, $NaBH_4$ (99%), were purchased from Aldrich. Zinc chloride, $ZnCl_2$ (99.99%), mercaptopropionic acid (MPA), and Se powder (>99.5%, 200 mesh) were obtained from Acros. Sodium hydroxide, NaOH, and ammonium hydroxide, NH_4OH (28−30%), were purchased from Mallinckrodt Chemicals. All chemicals were used without further purification. The H_2O used for QD synthesis was purified by a Barnstead NANOpure Infinity ultrapure water system.

Quantum Dot Preparation. MPA-QDs were prepared using a previously published protocol.[26] Briefly, fresh solutions of NaHSe were prepared by mixing $NaBH_4$ with H_2O followed by the addition of Se powder under an inert environment (N_2). The components reacted for ∼3.5 h, and then supernatants containing NaHSe were diluted to 20 mM using N_2-saturated H_2O. A solution of Cd-MPA was created by mixing MPA in H_2O with 5.0 mM $CdCl_2 \cdot 2.5\ H_2O$ stock solution, adjusting the pH to 9.5 using 1 M NaOH, and held at room temperature until needed. Last, a 60 mM $Zn(NH_3)_4^{2+}$ stock solution was prepared by dissolving $ZnCl_2$ in H_2O and titrating with NH_4OH, and was stored at 4 °C. Nucleation of CdSe dots occurred when the NaHSe stock was injected into Cd-MPA solution. This mixture was stirred for one hour prior to the addition of the $Zn(NH_3)_4^{2+}$ stock solution. These contents were then microwave irradiated (MARS5 microwave system, CEM Corp.) for 90 min at 150 °C. THIO-QDs were prepared through a ligand exchange using MPA-QDs. A 25 mM thiocholine solution was prepared by a hydrolysis reaction of acetylthiocholine chloride with 1 M NaOH. Progress of the hydrolysis reaction was monitored with an Accumet AB15 pH Meter (Fisher Scientific). Five hundred milligrams of acetylthiocholine chloride was dissolved in 80 mL of water and stirred. NaOH was added dropwise until the pH reached between 10 and 11. The pH decreased as hydroxide ions were consumed in the reaction, and more NaOH was added. This process continued until the pH stabilized. The final pH was adjusted to 9 using 1 M NaOH or HCl, and the final volume was adjusted to 100 mL. The MPA-QDs were placed in 12,000 molecular weight cutoff regenerated cellulose dialysis tubing (Fisher Scientific) and dialyzed in 3 L of water for several hours to remove MPA from the solution. The removal of MPA caused the quantum dots to aggregate and settle. The supernatant solution was removed and replaced by the thiocholine solution. This process was repeated twice, resulting in particles which had a positive zeta potential.

Characterization. *Spectroscopic Measurements.* All absorption measurements were obtained using a Shimadzu UV-2501PC UV−visible spectrometer. All emission measurements were obtained using a Horiba Jobin Yvon Fluorolog 3 fluorimeter.

The as-prepared quantum dot solutions (930 nM; concentration calculations were done using an extinction coefficient of 2.9×10^6 $cm^{-1}\ M^{-1}$ at 488 nm) was diluted 10:1 with purified water and placed in a quartz cuvette to measure the optical spectra. The excitation wavelength used for the emission spectrum was 375 nm, and all slits were set for a 2.5 nm band-pass.

To obtain a quantum yield measurement, the quantum dot solution was compared to a solution of rhodamine 6G. Both solutions were diluted to have an absorbance of 0.020 at a wavelength of 480 nm. At this wavelength and concentration, rhodamine 6G is known to have a quantum yield of 95%.[26] The peak emissions of both samples were measured with 480 nm excitation and the quantum yield calculated.

To determine possible time-dependent leaching of cadmium at a pH of 4.5, solutions of QDs (final concentration 466 nM) were adjusted to this pH using 1 M hydrochloric acid and left standing for different times. The samples were centrifuged using a Thermo-Fisher Scientific MX-150 ultracentrifuge at 150,000 rpm for 1 h, and the emission of the supernatant indicated that there were no QDs in solution. The cadmium concentration was determined using inductively coupled plasma mass spectroscopy (ICP-MS) by Galbraith Laboratories.

Size and Charge Measurements. Titrations of zeta potential and size vs pH were obtained using a Malvern Zetasizer Nano and an attached Malvern MPT-2 autotitrator. Zeta potential measurements were made using the method of phase analysis light scattering. Measurements were conducted at 25 °C at a forward scattering angle of 15°. Zeta potentials were calculated from the measured electrophoretic mobility using the Henry equation with a value of 1.5 for Henry's constant according to the Smoluchowski approximation. This approximation is consistent with the high dielectric constant of water.

Measurements were conducted at 25 °C with a backscattering angle of 273°. Dynamic light scattering results were analyzed using several algorithms. The data presented were analyzed using the constrained regularization method, CONTIN.[27] A quartic weighting scheme was used for multimodal analysis. CONTIN analysis provided the distribution of particle radii based on scattering intensity. In some cases, these were converted to relative volume distribution according to Mie theory and the known properties of the scattering material. The refractive index was set to 2.351, the value for ZnS at these conditions.[28]

Cell Culture. The murine alveolar macrophage cell line (MH-S) was purchased from the American Type Culture Collection (Manassas,

Va), and propagated using RPMI cell culture media (Gibco) supplemented with 10% fetal bovine serum (FBS, Atlanta Biologicals) and 0.1% penicillin−streptomycin (Gibco). Cells were passaged every 3−4 days and incubated at 37 °C with 5.0% CO_2. Cells were acclimated to these conditions for at least 12 h prior to QD exposure.

Biological Characterization and Internalization Mechanistic Assays. *Cytotoxicity and ELISA Experiments.* Cells were plated in 24 well plates at a density of 1×10^5 cells/well. Old media were aspirated, and QDs diluted to working concentrations using appropriate cell culture media were applied to the cell cultures and incubated for 24 h. Cells treated with 1% Triton-100 (Sigma) in complete culture media served as a positive control for lactate dehydrogenase (LDH) release assays, while cells treated with *E. coli* lipopolysaccharide (Sigma) served as the positive control for tumor necrosis factor-alpha (TNF-α) and interleukin-1beta (IL-1β) ELISAs. Additionally, to determine if toxicity was driven by the QDs themselves or residual ligand, QD suspensions were centrifuged at 150,000 rpm for 1 h, and QD supernatants were diluted 2-fold a total of 5 times using RPMI + 10% FBS cell culture media. Diluted supernatants were applied to macrophages, and the cells were incubated for 24 h. Cell supernatants were collected and assayed for necrosis using the LDH assay as a measurement of cell membrane permeability. The compatibility of QDs and QD supernatants in a cell-free system were also tested using the LDH assay to determine if the materials themselves interfere with the assay. In cellular exposure experiments, cell supernatants were collected from each well and clarified by centrifugation and transferred to clean microfuge tubes and stored at −80 °C until analysis for cytokine secretion or LDH release. All experiments were performed at least 3 times.

LDH Cell Viability Assays. Cellular supernatants were pipetted in duplicate into flat bottom 96-well plates and assayed for LDH activity using kits from Clontech per manufacturer's instructions. Optical densities (ODs) representing enzyme activity were measured colormetrically using a BMG LabTech Omega plate reader at an absorbance wavelength of 490 nm and a reference wavelength of 600 nm. Cell viability was calculated using the following equation:

$$\%\text{Cell Death} = \frac{\text{mean OD experimental} - \text{mean OD negative control}}{\text{mean OD positive control} - \text{mean OD negative control}} \times 100$$

ELISAs. TNF-α and IL-1β secretion was measured via ELISAs using DuoSets purchased from R&D Systems according to the manufacturer's recommendations. Supernatants were assayed in duplicate, and plates were read using a BMG LabTech Omega plate reader at an absorbance wavelength of 450 nm with a correction wavelength of 570 nm. Experimental sample concentrations were calculated with Omega software using a four parameter logistic standard curve.

Flow Cytometry. All flow cytometry experiments were performed in triplicate. Cells were seeded in 6-well plates (Corning) at a density of 1.5×10^6 cells/well and allowed to adhere overnight prior to QD exposure. Flow cytometry staining procedures are described below.

Annexin V Staining. Cells were exposed to QDs for 24 h. Cells were then washed with PBS three times prior to being harvested by trypsinization. Cell concentration was adjusted to 1×10^6 cells per tube, and cells were resuspended in 100 μL of Annexin binding buffer (Invitrogen); 5 μL of Annexin V-APC (BD Biosciences) was then added to each tube. Tubes were incubated in the dark at room temperature for 15 min before an additional 400 μL of binding buffer was added. Cells were analyzed for fluorescence using a FACScalibur flow cytometer at an excitation wavelength of 488 nm for detection of QDs and 635 nm for Annexin-APC.

Scavenger Receptor Competition Assay. Three types of culture media were used: RPMI only, RPMI containing 10% FBS and X-VIVO 15 serum-free, phenol red-free media (Lonza). Culture media were removed and replaced with each of the fresh media listed above containing 100 μg/mL of Poly /inosinic acid (Poly-I), a nonspecific scavenger receptor ligand, for 30 min. This concentration of Poly-I was nontoxic to the cells over a 24 h period as assayed by LDH release and Annexin V staining. QDs were suspended in fresh media containing 100 μg/mL Poly-I and then applied to macrophages. Unexposed cells and cells treated with Poly-I only served as controls. Cells were incubated for 6 h, then harvested and analyzed for fluorescence by flow cytometry using a FACScalibur flow cytometer at an excitation wavelength of 488 nm.

Endocytosis Inhibition. Cells were pretreated for 30 min with fresh media (RPMI + FBS) containing cytochalasin D (2.5 μg/mL), which inhibits actin polymerization, 50 μM of chlorpromazine, a clathrin inhibitor, or 50 μM nystatin, a caveolae inhibitor. All inhibitors were purchased from Sigma and diluted to nontoxic (as tested by LDH release and Annexin V staining) working concentration using PBS. Cells that were not exposed to QDs and cells treated with inhibitors only served as controls. After pretreatment, media were removed and replaced with media containing the inhibitor and increasing concentrations of QDs. Cells were incubated with or without inhibitor and with or without QDs for 2 h, then washed 3 times with PBS. Cells were harvested by trypsinization, suspended in HBSS and analyzed by flow cytometry using a FACS calibur flow cytometer at an excitation wavelength of 488 nm.

Live Cell Imaging. Cells were plated on glass coverslips situated in 35 mm Petri dishes at a density of 5×10^4 cells/coverslip and incubated overnight. Prior to live cell imaging and QD addition, cells were incubated with phenol red-free, serum-free X-VIVO media containing 25 nM LysoTracker Red (Invitrogen) for at least 15 min. QDs (final concentration of 75 nM) were added following 3 min of image collection. Images were acquired sequentially at an excitation of 442 nm, dichroic 442/488/565/643 and emission (barrier) 488/565/643 for QDs, while LysoTracker Red was detected using an excitation wavelength of 561 nm, a dichroic setting of 442/488/565/643 and a barrier setting of 488/565/643 every 6 s for a total of 20 min. In additional experiments, cells were incubated with LysoTracker Red and QDs for 45 min prior to image collection. Images were acquired using a Hamamatsu C9100 EM-13 camera connected to a Visitech Infinity3 2D array scanning multibeam confocal scanner and an IX81 microscope equipped with a 100×, 1.40 N.A. UPlanApo objective lens. Movies were constructed using MetaMorph software (Molecular Devices) using image stacks that were background subtracted with the statistical correction option of the "Background and Shading Correction" application. Out of focus images were removed prior to the production of movies. See Supporting Information for information regarding colocalization analyses.

Statistical Analysis. Comparisons between QD treatments were analyzed for statistical significance using One-way ANOVA performed with SigmaPlot software.

RESULTS

QD Characteristics. The microwave-based synthesis procedure for the QDs used in this study has been reported previously.[26] These QDs contain a CdSe core with a CdS intermediate shell followed by a ZnS outer shell. MPA-QDs were capped with 3-mercapatopropionic acid (3-MPA). Detailed chemical and physical characterization of these MPA-QDs has been reported, including composition, size, and morphology.[26] THIO-QDs were derived from the same core−shell QDs as the MPA-QDs by a ligand exchange process where MPA was replaced with thiocholine. Since the THIO-QDs were derived from the same core−shell QDs as the MPA-QDs and capped by a ligand exchange process, they had comparable, emission, absorption spectra, and quantum yields as the previously reported MPA-QDs.[26]

Figure 1A illustrates the particle sizes and zeta potential of the MPA-QDs as a function of pH in aqueous solution. The size data in this figure are reported as average diameters based on the intensity distribution (later we use volume distributions for the media dispersed samples; our purpose in Figure 1 was to

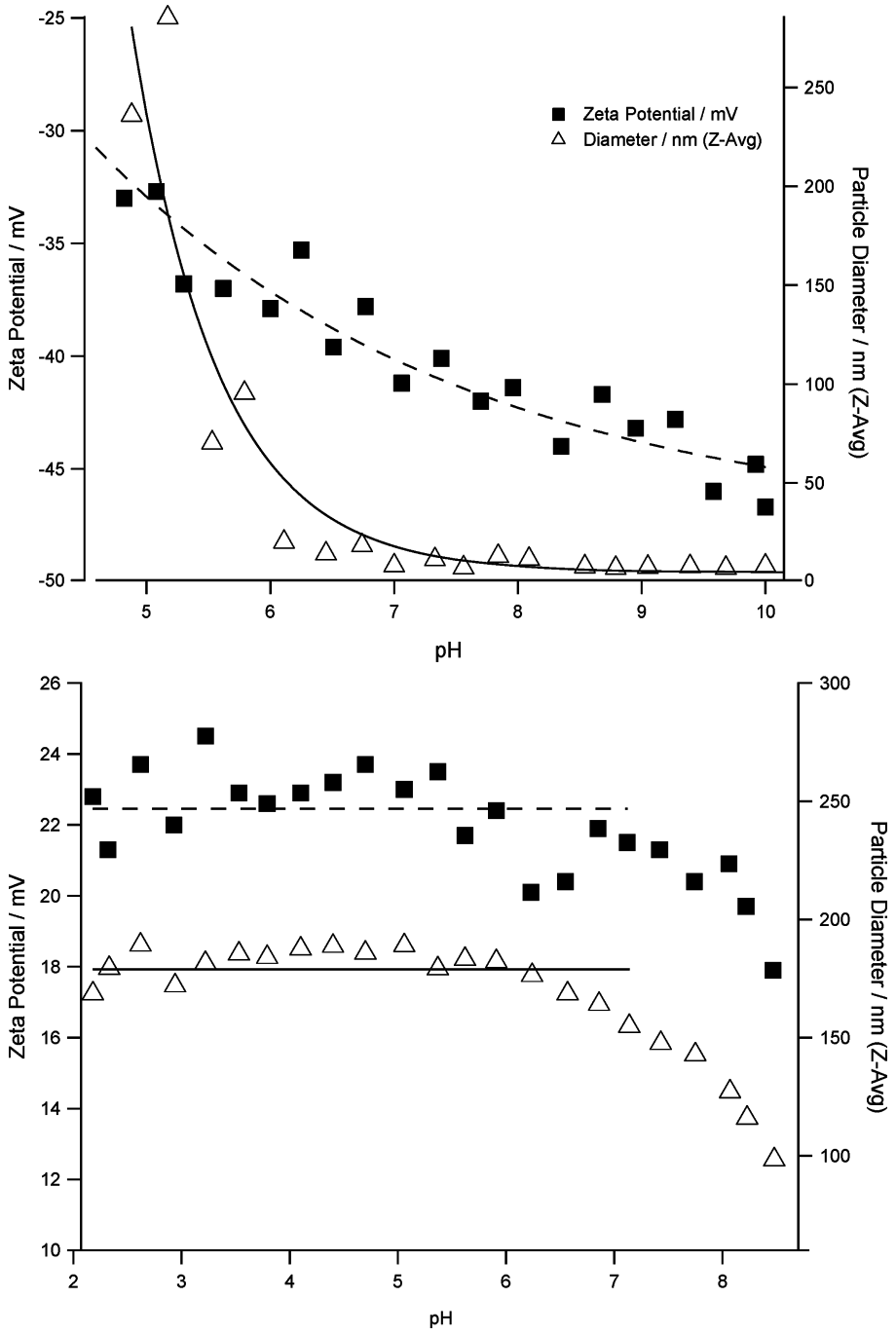

Figure 1. Chemical characterization of QDs. Plots of MPA-QD (top panel) and THIO-QD (bottom panel) Z-average diameter and zeta potential as a function of pH. QD concentrations for size titration were 931 nM and 186 nM for zeta potential.

examine the aggregation characteristics in water as a function of pH). The hydrodynamic diameter for MPA-QDs is relatively constant between pH 5.5−11 and shows a marked increase below pH ∼6, indicating aggregation. The zeta potential remains negative throughout the pH titration, with a gradual increase in the zeta potential from −48 mV at pH 10 to −34 at pH 4.5. The behavior of the THIO-QDs in water is shown in Figure 1B. The zeta potential was found to remain positive over pH of 2−7 and decreased at higher pH. Thus, as synthesized, the MPA-QDs and THIO-QDs maintain a negative and positive charge, respectively, over biologically relevant pH ranges in water.

Three media types were examined in this study: RPMI without supplements, RPMI + fetal bovine serum (FBS), and X-VIVO serum-free, phenol red-free media. Dynamic light scattering and zeta potential of all three media were examined and reported in Table 1, and the raw data is in the Supporting Information. The analysis of light scattering data used the volume distribution rather than the intensity since large particles scatter more, and volume (or number) distribution is a better measurement of size. All three media had particles with diameters ranging from 1 to 8 nm. Additionally, in all three media types, the zeta potential data was noisy (Supporting Information) due to the small size of the particles

dx.doi.org/10.1021/tx2003195 | *Chem. Res. Toxicol.* 2011, 24, 2176−2188

Table 1. Volume-Based Diameters and Zeta Potentials for MPA-QDs and THIO-QDs in Media with and without Poly-I[a]

MPA-QDs				THIO-QDs				
− Poly I		+ Poly I		− Poly I		+ Poly I		
size (nm)	charge (mV)	size (nm)	charge (mV)	size (nm)	charge (mV)	size (nm)	charge (mV)	
8, 26	−34	17	−26.6	20, 62	15	18, 42, 77, 450, 2700	−24.6	RPMI
54	−15	25	−20.3	140, 1200	−11	62, 504	−17.3	RPMI + FBS
12, 39	−24	30	−14.8	3000	0	1300	0	X-VIVO

[a]All of the experimental data corresponding to numbers in this table are provided in the Supporting Information, Figures 1−34.

and not readily amenable to interpretation. The size and charge of the two QDs were examined in these three media types, in the presence and absence of Poly-I, and the data are summarized in Table 1. Also, the Supporting Information shows the actual distribution curves obtained from the light scattering and the raw zeta potential data for QDs in all media. The THIO-QDs and MPA-QDs behaved differently in each media. As synthesized, MPA-QDs had a diameter of ∼26 nm and charge of −44 mV (pH 9). Note that these sizes differ slightly from Figure 1 since it is the volume-based number that is being used henceforth. Also, our previous TEM studies show that the QDs are about 5.3 nm in diameter, so the light scattering data indicates that there is some aggregation even in water.[26] Upon replacing MPA with thiocholine, the size was 17 nm with a charge of +34 mV (pH 9). When suspended in all three media types, the MPA-QDs exhibited a stable, optically clear dispersion. In RPMI, the size distribution was bimodal: ∼8 and 26 nm with a charge of −34 mV. Smaller sized particles of ∼1 nm were present in RPMI alone. It is unclear if these contribute to the ∼8 nm particles. In RPMI + FBS, the size of the MPA-QDs was 54 nm, and the charge was −15 mV. In X-VIVO media, the size distribution for MPA- QDs was also bimodal: ∼12 and 39 nm, with a negative charge of −24 mV. The X-VIVO media by itself had particles with sizes of ∼7 nm and is possibly the contributor to the smaller of the two sizes in the bimodal distribution. Thus, in both RPMI + FBS and X-VIVO media, the QDs are increasing significantly in size, more so in the former, possibly by association with proteins, which also leads to lowering in the surface charge.

A stable, optically clear dispersion of THIO-QDs was achieved only with RPMI. The size distribution in RPMI was bimodal with ∼20 and ∼62 nm particles, and the surface charge was +15 mV. In RPMI + FBS, the solution turned cloudy with time (15−30 min) and is reflected in the broad particle size distribution with peaks at 140, 1200 nm, and also larger aggregates. The zeta potential of THIO-QDs in RPMI + FBS was −11 mV. With the X-VIVO media, aggregation for THIO-QDs was more marked with sizes over a range of 1000−6000 nm (average around 3000 nm), and the particles had a neutral charge of ∼0 mV, also indicating association of negatively charged species from the media with THIO-QDs.

To simulate the acidic environment of the lysosome, QDs were incubated at a pH of 4.5 in water (466 nM) under ambient conditions, and the concentration of free Cd^{2+} in solution was determined by ICP-MS. In the case of MPA-QDs, the concentration of Cd^{2+} was not detectable after 15 min and increased to 1.8 μM over 24 h, whereas for the THIO-QDs, the Cd^{2+} content increased from 0.9 μM after 15 min to 3.6 μM after 24 h at pH 4.5.

Cytotoxicity and Proinflammatory Response of QD Exposed Cells. We incubated cells with QDs with concentrations as high as 500 nM, though previous studies have shown that 20 nM concentration is suitable for imaging.[23,26] At a concentration of 500 nM MPA-QDs, greater than 40% of cells were found to be necrotic, (Figure 34, Supporting Information), so for detailed necrosis and apoptosis measurements, we limited the concentration of QDs to 125 nM. These experiments were carried out in RPMI + FBS since it closely simulates physiological conditions. Both MPA-QDs and THIO-QDs are stabilized by ligands, an excess of which is present in the QD suspension. For the LDH assay, which is a measure of necrosis, both the supernatants of the QDs and the entire QD suspension were examined. It is also relevant to point out that the supernatant from the THIO-QDs interfered with the LDH assay at 250 nM and higher concentrations. Figure 2 shows the

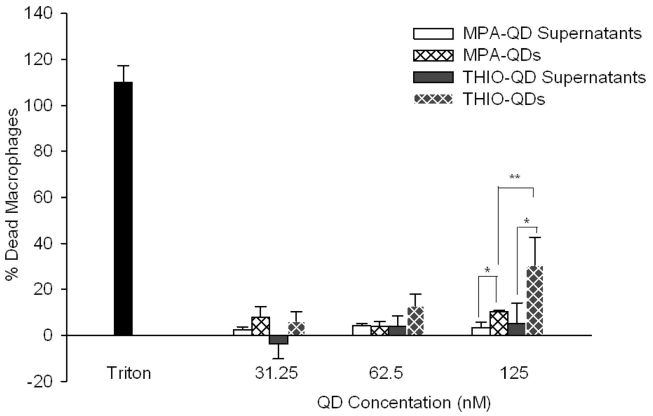

Figure 2. Necrosis induced by MPA-QDs, THIO-QDs, and QD supernatants in murine alveolar macrophages. Cells were incubated with increasing concentrations of MPA-QDs, THIO-QDs, and equivalent QD supernatants containing excess ligand. QDs and QD supernatants were diluted in RPMI + FBS and exposed to macrophages for 24 h before cellular necrosis was measured via LDH release. THIO-QDs were significantly more toxic ($p < 0.01$, indicated by **) than MPA-QDs at 125 nM. MPA QDs were significantly more toxic than MPA-QD supernatants at 125 nM ($p < 0.05$ indicated by *), and THIO-QDs were significantly more toxic than THIO-QD supernatants at 125 nM ($p < 0.05$, indicated by *). Error bars are the standard deviation from 3 independent experiments.

LDH assay data for both MPA-QD, THIO-QD, and their supernatants. Dose-dependent necrosis of cells is observed for the QD suspensions, while the supernatants exhibited little toxicity, at the level of ∼5% death of cells. The THIO-QDs were significantly more cytotoxic at 125 nM ($p < 0.01$), with 30% cell death as compared to MPA-QDs.

Annexin V staining was performed after a 24 h exposure to examine the apoptotic response of cells exposed to QDs suspended in RPMI + FBS media. Macrophages exposed to 250 nM of MPA-QDs or less were observed to have between a 10 to 15% increase in the number of apoptotic cells compared to that of unexposed cells (Figure 3A), while cells treated with

dx.doi.org/10.1021/tx2003195 | Chem. Res. Toxicol. 2011, 24, 2176−2188

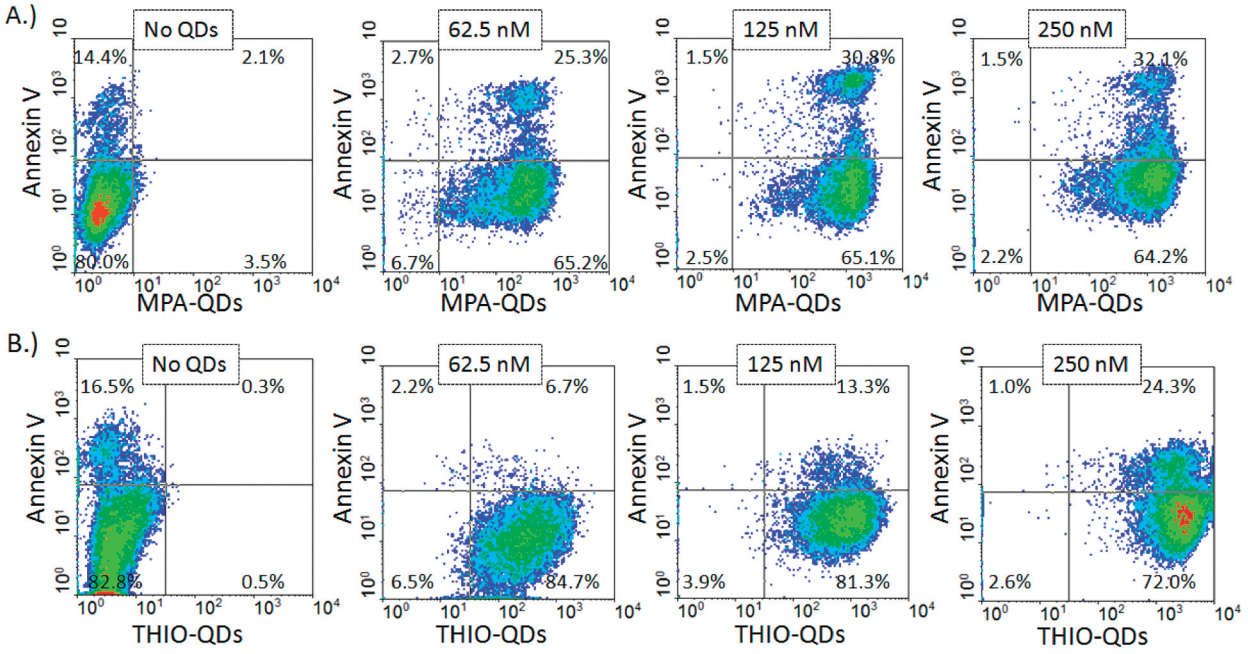

Figure 3. Apoptotic effects of MPA-QDs and THIO-QDs in murine alveolar macrophages after 24 h. (A) Macrophages were incubated with increasing concentrations of MPA-QDs suspended in RPMI + FBS, and apoptosis was measured via flow cytometry. The number of apoptotic cells approximately doubled for concentrations up to 250 nM. (B) Macrophages were incubated with increasing concentrations of THIO-QDs suspended in RPMI + FBS, and apoptosis was measured via flow cytometry. Numbers of apoptotic cells increased in a dose dependent manner. Figures are representative of three independent experiments for each QD type.

500 nM were found to have ~3.5 times (56.8%) as many apoptotic cells, indicating that the mechanism of cytotoxicity is apoptosis (Figure 35, Supporting Information). A dose dependent increase in Annexin V staining for cells incubated with THIO-QDs was observed, where macrophages exposed to 62.5, 125, or 250 nM THIO-QDs resulted in 6.7%, 13.3%, and 24.3% Annexin V positive cells, respectively (Figure 3B).

Levels of secreted TNF-α and IL-1β in supernatants recovered from macrophages exposed to MPA-QDs and THIO-QDs suspended in RPMI + FBS were quantified by ELISA. Macrophages treated with 100 ng/mL of lipopolysaccharide alone resulted in TNF-α levels greater than 175 pg/mL (data not shown) indicating that these cells are capable of producing a proinflammatory response. Supernatants derived from cells incubated with QDs for short periods (2 h) did not result in proinflammatory cytokine induction (data not shown); thus, samples were collected after 24 h exposures. TNF-α levels range from undetectable for untreated cells and cells treated with 62.5 and 125 nM of MPA-QDs. The amounts of TNF-α secreted from macrophages after exposure to MPA-QDs were significantly different from amounts secreted from cells exposed to THIO-QDs (Figure 4). Supernatants from cells treated with 500 nM of MPA-QDs show an increase of 33 ± 8 pg/mL of TNF-α compared to 23 ± 4 pg/mL from cells treated with 250 nM of MPA-QDs. These same supernatants were also analyzed for IL-1β, which was undetectable (data not shown). Supernatants collected from cells treated with 250 nM of THIO-QDs secreted 51 ± 12 pg/mL of TNF-α but only 6 ± 11 pg/mL after exposure to 500 nM of THIO-QDs (40% cell death at these high concentrations).

Internalization, Intracellular Localization, and Mechanism of QD Uptake. There are several possible mechanisms that facilitate endocytosis, including internalization through caveolae and clathrin coated pits. We used an inhibitor

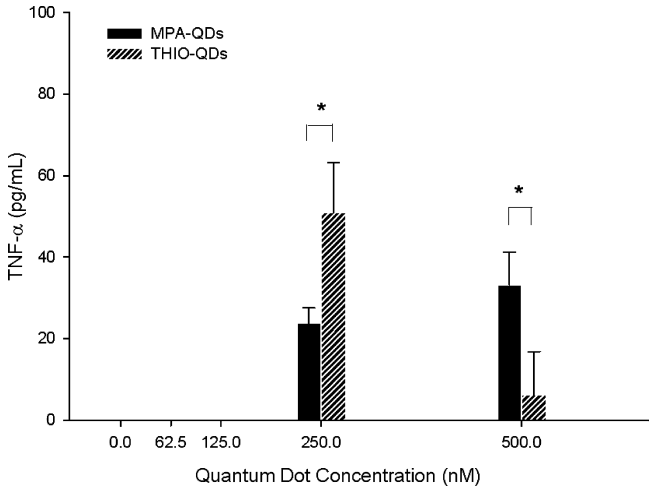

Figure 4. Secretion of TNF-α from macrophages exposed to MPA-QDs and THIO-QDs. Significant differences ($p < 0.001$, $n = 3$, as indicated by *) in TNF-α secretion levels were measured using ELISA from cell supernatants after exposure to MPA-QDs and THIO-QDs suspended in RPMI + FBS for 24 h.

approach to block internalization of MPA-QDs, all experiments being carried out in RPMI + FBS media. Initially, cells were pretreated with cytochalasin D (inhibits actin polymerization and phagocytosis), nystatin (binds cholesterol and disrupts caveolae coat structure), or chlorpromazine (prevents clathrin recycling) prior to the addition of MPA-QDs suspended in media containing inhibitors. Neither nystatin treated cells nor cytochalasin D treated cells displayed a reduction in fluorescence after exposure of cells to MPA-QDs suspended in the corresponding inhibitor (data not shown). However, in cells treated with chlorpromazine, fluorescence is substantially reduced at all concentrations tested (Figure 5A and B).

dx.doi.org/10.1021/tx2003195 | Chem. Res. Toxicol. 2011, 24, 2176–2188

Macrophages exposed to 150 nM MPA-QDs in the presence of chlorpromazine exhibited approximately 66% less fluorescent positive cells. Likewise, when macrophages were exposed to 125 nM THIO-QDs in the presence of chlorpromazine, ~60% less fluorescent cells was observed compared to that in controls. Differences in fluorescence after treatment with the clathrin inhibitor are summarized in Figure 5 and Table 2.

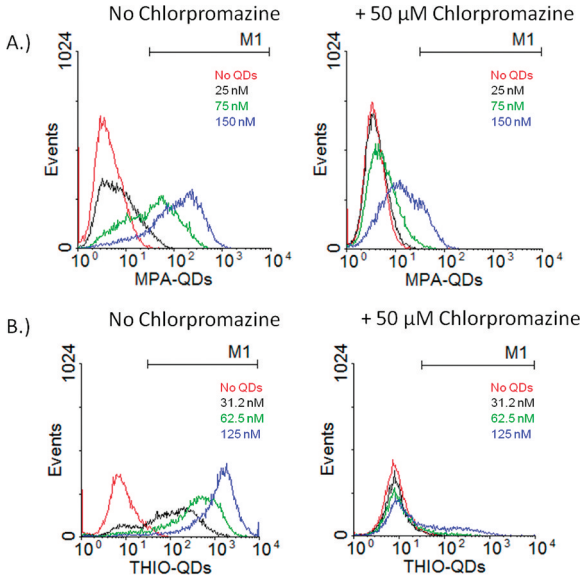

Figure 5. Role of clathrin-coated pits in QD internalization. (A) Macrophages were exposed to MPA-QDs alone suspended in RPMI + FBS (left panel) or pretreated with chlorpromazine (50 μM) for 30 min prior to exposure to MPA-QDs suspended in RPMI + FBS containing chlorpromazine (right panel). (B) Macrophages were exposed to THIO-QDs alone suspended in RPMI + FBS (left panel) or pretreated with chlorpromazine (50 μM) for 30 min prior to exposure to THIO-QDs suspended in RPMI + FBS containing chlorpromazine (right panel).

Table 2. Percent Fluorescent Cells Exposed to Negative and Positive QDs Suspended in RPMI + FBS in the Absence and Presence of the Clathrin Inhibitor, Chlorpromazine[a]

	% fluorescent cells	
MPA-QD concentration (nM)	− chlorpromazine	+ chlorpromazine
0	0.8 ± 0.0	0.5 ± 0.4
25	9.5 ± 2.3	0.4 ± 0.1
75	63.1 ± 2.5	3.2 ± 0.3
150	87.4 ± 2.5	29.9 ± 6.1
	% fluorescent cells	
THIO-QD concentration (nM)	− chlorpromazine	+ chlorpromazine
0	1.0 ± 0.2	1.4 ± 0.3
31.2	65.6 ± 2.4	2.8 ± 0.5
62.5	85.1 ± 1.6	9.9 ± 1.4
125	91.5 ± 1.5	26.8 ± 3.6

[a]Values are the average of 3 independent experiments ± standard deviation.

Using live cell confocal imaging, we observed MPA-QDs localizing to the cell membrane within minutes (3 min) after they were introduced to the culture, followed by their appearance in intracellular vesicles (9 min) and mature vesicles at 12 and 17 min (Figure 6A–E). All experiments were

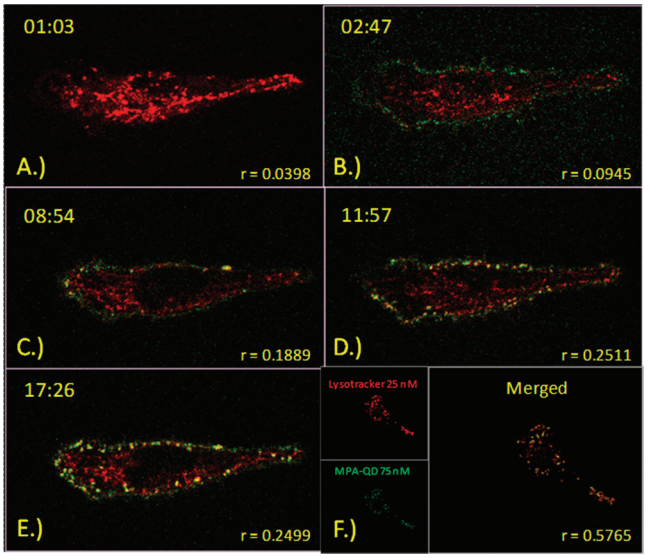

Figure 6. MPA-QD compartmentalization in macrophages. (A) Macrophages stained with LysoTracker Red just prior to the addition of MPA-QDs suspended in serum free, phenol red-free X-VIVO media. (B) MPA-QDs form a halo around the outside of the cell within 2 min. (C) Yellow vesicles indicative of colocalization are apparent after ~9 min. (D) MPA-QDs are clearly in acidic compartments by 12 min. (E) Vesicles begin to track in the cell by 17 min postexposure. In panel F, macrophages were incubated with LysoTracker followed by the addition of 150 nM MPA-QD (final concentration = 75 nM) for 45 min prior to imaging. The majority of QDs are found within lysosomes. *r* is the correlation between MPA-QDs and LysoTracker.

performed in X-VIVO serum-free, phenol red free media due to the interference of phenol red with imaging. We stained acidic organelles using LysoTracker Red to visualize the late endosomal pathway and were able to localize MPA-QDs in the lysosomes within 20 min of their introduction into live cultures (Supporting Information). The image presented in Figure 6F is representative of QD/lysosomal colocalization after 45 min of incubation from the second movie file in Supporting Information. We quantified the amount of colocalization in this cell over time, and MPA-QDs were found to have a correlation coefficient (*r* value) of 0.577 ± 0.066, indicating that the majority of QDs are retained in acidic compartments. Colocalization of MPA-QDs and LysoTracker is consistent with transport through the endosomal pathway to the lysosomes.

THIO-QDs were also observed to be internalized. However, flow cytometry data collected from the clathrin inhibition assays indicate cellular association occurred within 2 h, in contrast to MPA-QDs which were internalized in approximately 20 min. Their compartmentalization in lysosomes could not be definitively established since the aggregated QDs in serum free media scatter the laser light (561 nm), making it difficult to distinguish from the LysoTracker Red signal. This phenomenon was not apparent for MPA-QDs, which remained dispersed in the media.

To identify a possible mechanism of QD internalization in all three media types, we evaluated the molecular relationship between scavenger receptors and charged QDs using a competition assay using Poly-I, a nonspecific scavenger receptor ligand. When cells were incubated with MPA-QDs suspended in all media types containing 100 μg/mL Poly-I, a

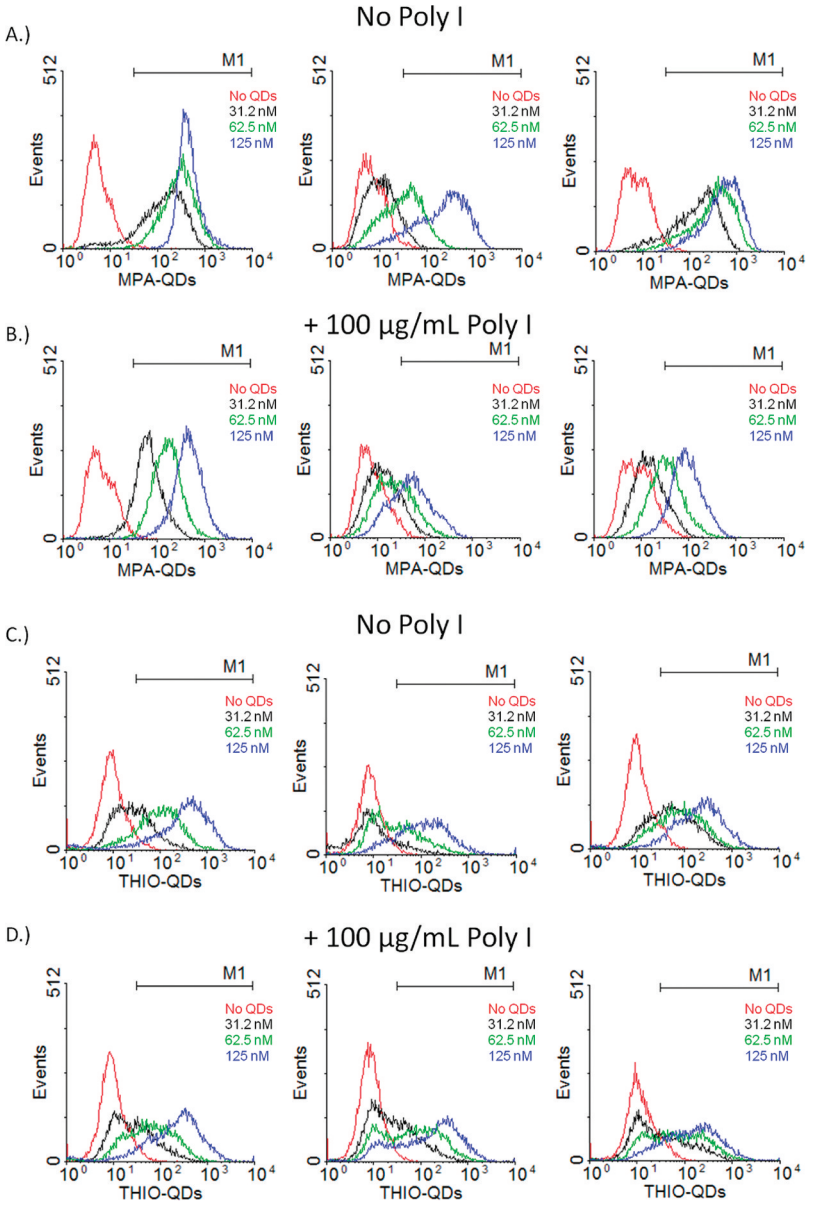

Figure 7. Comparisons in QD charge and macrophage scavenger receptor association. (A) Macrophages were treated with increasing concentrations of MPA-QDs suspended in RPMI (left panel), RPMI + FBS (middle panel), or X-VIVO media (right panel) for 6 h prior to analyses of cellular fluorescence by flow cytometry. (B) Macrophages were pretreated with RPMI (left panel), RPMI + FBS (middle panel), or X-VIVO media containing Poly-I (100 μg/mL) for 30 min. MPA-QDs suspended in each media type containing Poly-I were added to the cells and incubated for 6 h prior to analyses of cellular fluorescence by flow cytometry. (C) Macrophages were treated with increasing concentrations of THIO-QDs suspended in RPMI (left panel), RPMI + FBS (middle panel), or X-VIVO media (right panel) for 6 h prior to analyses of cellular fluorescence by flow cytometry. (D) Macrophages were pretreated with RPMI (left panel), RPMI + FBS (middle panel), or X-VIVO media containing Poly-I (100 μg/mL) for 30 min. THIO-QDs suspended in each media type containing Poly-I were added to the cells and incubated for 6 h prior to analyses of cellular fluorescence by flow cytometry.

reduction in fluorescence, indicating lower association of QDs with cells, was apparent particularly at lower MPA-QD concentrations (Figure 7A,B and Table 3). However, there are differences between the media. At MPA-QD concentrations of 31.2 and 62.5 nM, fluorescence was lower for MPA-QDs suspended in RPMI + FBS (15.4 ± 0.5% and 29.8 ± 4.0%, respectively) compared to those suspended in RPMI (79.4 ± 2.5% and 92.0 ± 1.6%, respectively) and X-VIVO media (78.1 ± 3.4% and 87.4 ± 3.1%, respectively), indicating that serum constituents in FBS are preventing QDs from associating with macrophages. Nevertheless, in the presence of Poly-I, a decrease in fluorescence is evident in all cases, especially for QD concentrations less than 100 nM. Table 1 shows that the MPA-QDs do not have major interactions with Poly-I, and the QDs remain negatively charged and with sizes <30 nm. When suspended in different types of biological media, THIO-QDs exhibited a wide range of sizes and negative, positive, or neutral charge; nonetheless, they did not appear to associate with scavenger receptors in the conditions tested (Figure 7C and Table 3). Macrophages exposed to THIO-QDs suspended in media containing Poly-I did not exhibit reduced fluorescence but rather an increase in fluorescence (Figure 7D and Table 3). Table 1 shows clearly that in RPMI, the positively charged QDs revert to negative surface charge in the presence of Poly-I and also form larger

dx.doi.org/10.1021/tx2003195 | Chem. Res. Toxicol. 2011, 24, 2176–2188

Table 3. Percent Fluorescent Cells Exposed to Negative or Positive QDs Suspended in RPMI, RPMI + FBS, or X-VIVO Media in the Absence and Presence of the Scavenger Receptor Inhibitor, Poly-I[a]

	% fluorescent cells					
	RPMI		RPMI + FBS		X-Vivo	
MPA-QD concentration (nM)	− Poly I	+ Poly I	− Poly I	+ Poly I	− Poly I	+ Poly I
0	0.7 ± 0.1	0.5 ± 0.2	0.7 ± 0.3	1.0 ± 0.3	0.7 ± 0.3	1.1 ± 0.3
31.2	79.4 ± 2.5	54.0 ± 4.0	15.4 ± 0.5	5.6 ± 0.4	78.1 ± 3.4	7.5 ± 1.5
62.5	92.0 ± 1.6	75.9 ± 2.4	29.8 ± 4.0	17.3 ± 2.0	87.4 ± 3.8	27.3 ± 2.6
125	95.2 ± 1.8	96.4 ± 1.6	82.8 ± 5.6	42.2 ± 3.4	96.5 ± 0.5	70.0 ± 7.0
	RPMI		RPMI + FBS		X-Vivo	
THIO-QD concentration (nM)	− Poly I	+ Poly I	− Poly I	+ Poly I	− Poly I	+ Poly I
0	1.6 ± 0.2	1.3 ± 0.5	0.7 ± 0.1	0.7 ± 0.3	2.4 ± 0.9	1.7 ± 0.2
31.2	27.7 ± 6.5	33.8 ± 8.2	9.8 ± 1.7	23.3 ± 5.3	32.1 ± 0.6	50.2 ± 4.0
62.5	67.1 ± 0.7	60.9 ± 12.7	24.3 ± 6.2	49.6 ± 5.8	40.1 ± 11.5	66.8 ± 6.3
125	81.0 ± 3.5	82.6 ± 2.4	57.6 ± 14.3	69.1 ± 5.1	65.7 ± 6.4	85.6 ± 2.5

[a]Values are the average of 3 independent experiments ± standard deviation.

aggregates, indicating a strong interaction of THIO-QDs with Poly-I. In the other two media, the THIO-QDs are either negatively charged or neutral and form large aggregates and in the presence of Poly-I; there are some changes, but nothing as dramatic as those observed in RPMI.

DISCUSSION

This discussion is based on the profound influence of QD charge and aggregation characteristics in different biological media which affects their subsequent cytotoxicity and interactions with macrophages.

QD Characteristics. The negative QDs in this study had a CdSe core with a CdS/ZnS shell and were capped with MPA. The carboxylate groups on MPA gave QDs a negative zeta potential (Figure 1A). 3-MPA has a pK_a of 4.4,[29] and as protonation of the carboxylate groups proceeds, aggregation of the QDs occurs,[30] indicating that the repulsion between the negative charges keeps the colloid stable at high pH. In all three culture media examined in this study, the MPA-QDs remained dispersed, and the solutions were free of visible aggregation. Light scattering indicated a particle size range of 8−54 nm (Table 1), and the zeta potential remained negative, though it decreased from −44 mV in water to −34, −15, and −24 mV in RPMI, RPMI + FBS, and serum-free media.

The behavior of THIO-QDs is unlike MPA-QDs in that they are far more susceptible to aggregation in media. In water (pH 2−7), THIO-QDs maintain a positive zeta potential because of the quaternary nitrogen functionality. The THIO-QDs formed large aggregates in the RPMI + FBS and X-VIVO media, whereas 20 and 62 nm particles were found in RPMI. The zeta potential was positive for RPMI (15 mV) and almost neutral for X-VIVO media (∼0 mV). In the case of RPMI + FBS, the zeta potential became negative (−11 mV). Recent studies investigating the interactions of nanoparticles in biological media have revealed that protein coronas form.[31,32] Indeed, work by Warnement et al.[33] definitively established the association of QDs with serum albumin using polyacrylamide gel electrophoresis and that these interactions can interfere with QD and specific cell surface receptor targeting. Further, CdSe/ZnS QDs stabilized with 11-mercaptoundecanoic acid formed stable complexes with sheep serum albumin and were also found to exhibit photostability over several days, even though they were confined to the acidic lysosomal compartment.[34] Protein corona formation inherently influences nanoparticle charge; when nanoparticles containing amine groups were suspended in PBS buffer, a negative charge was recorded.[31] Amine modified polystyrene spheres also exhibited a switch of surface charge from positive to negative in cell culture media due to binding of serum proteins.[35] In the current study, as-synthesized positively charged THIO-QDs suspended in media (RPMI + FBS or X-VIVO) also switched to negative or neutral zeta potential, which we attribute to the formation of protein coronas on the QD surface. We conclude that negatively charged nanoparticles retain their approximate size and charge in biological media, whereas positively charged nanoparticles become negatively charged or neutral with significant aggregation.

The marked difference in aggregation between the negatively and positively charged QDs in media and with Poly-I can be understood based on simple electrostatic arguments. At physiological pH, there are considerably more negatively charged molecules (primarily due to carboxylates), which, because of electrostatic repulsions, do not interact with the negatively charged MPA-QDs. However, these species can bind to the positively charged THIO-QDs. Upon binding, the positive charge on the QD surface decreases, thereby decreasing inter QD repulsions and leads to aggregation. Eventually, these aggregates can become negatively charged (RPMI + FBS or with Poly-I) or remain neutral (X-VIVO), but once the aggregates are formed, they are not easily dispersed without external forces.

Positively and Negatively Charged QD Cytotoxicity. We sought to compare the cytotoxic effects of MPA-QDs and THIO-QDs. These experiments were performed in RPMI + FBS experiments where both the MPA-QDs and THIO-QDs are negatively charged, with MPA-QD sizes of ∼20 nm and THIO-QDs forming large aggregates of ∼1200 nm. Lovrić et al.[21] determined that the mechanism of MPA-capped QD cytotoxicity (1−10 μg/mL) in MCF-5 breast cancer cells was due to the formation of reactive oxygen species (ROS). Chan et al.[36] further established that ROS generated in neuroblastoma cells following exposure to QDs with a CdSe core (150 to 300 nM) induced apoptosis via activation of JNK-mediated signaling. These investigators also determined that cell death could be prevented by capping CdSe QDs with a ZnS shell. It has been proposed that mechanisms of QD cytotoxicity (187.5 nM to 3 μM) are due to both the formation of ROS and Cd^{2+} leaching.[37] Other studies corroborate this finding; in

dx.doi.org/10.1021/tx2003195 | Chem. Res. Toxicol. 2011, 24, 2176−2188

particular, one group found that CdS QD cytotoxicity (10−80 μg/mL) is dependent on size and that the mechanism of toxicity shifts from ROS driven to Cd^{2+} dependent as QD concentration was increased.[38] It is established that cadmium related ROS generation can induce apoptosis at 10 to 50 μM.[39] The dissolution of QDs at acidic pH within the lysosome is a source of Cd^{2+}. While we did not measure the formation of ROS in the current study, elemental analysis indicated concentrations of 1.8 μM Cd^{2+} from a MPA-QD suspension and 3.6 μM from a THIO-QD suspension at pH 4.5 (starting concentration of 466 nM) after a 24-h period. Thus, in the current study, the toxicity of QDs can be attributed to leached Cd^{2+} that occurs in acidic conditions present in the lysosomal compartment. Our results are in agreement with those of Derfus et al.[40] who investigated the role of surface coating CdSe QDs with ZnS shells and also bovine serum albumin QD induced cytotoxicity. The oxidation of QDs resulted in the leaching of free Cd^{2+} from the QD core, which correlated with increased cytotoxicity. The addition of surface coatings was found to reduce cytotoxicity in hepatocytes but not eliminate cytotoxicity altogether.[40] Supernatants collected from QD suspensions after centrifugation exhibited little toxicity (Figure 2). Other research has found that capping agents alone can induce genotoxicity; Hoshino et al.[41,42] found that mercaptoundecanoic acid, a common capping agent providing nanoparticles with negative charge, induced significant DNA damage in WTK-1 cells.

Proinflammatory Properties of QDs. The MH-S macrophage cell line is capable of phagocytosing particles and releasing proinflammatory cytokines upon stimulation[43] and has been shown to generate a proinflammatory response after exposure to silica particles.[44] When the cells were stimulated with LPS (100 ng/mL), it resulted in 198.3 pg/mL of TNF-α (data not shown). Thus, we sought to determine if QDs were capable of inducing a proinflammatory response in this cell line. There is no increase in TNF-α release in cells exposed to concentrations less than125 nM. Very large concentrations of QDs (250 or 500 nM), which caused cell necrosis, also led to the release of TNF-α. The upregulation of proinflammatory cytokines in response to QD exposure has not been fully examined. However, one study by Lee et al.[45] found that QDs (0.2−25 nM) induced the upregulation of TNF-α and CXCL-8, which correlated with ROS formation, while another study demonstrated that cadmium alone (50 μM) resulted in the upregulation of IL-8 in intestinal cells, yet TNF-α and interferon-γ levels remained unchanged.[46] The confinement of QDs in the acidic environment of the lysosome causes destabilization of QDs and the release of Cd^{2+} from the inner shell and core, contributing to cell death. The cytotoxic and inflammatory behavior after exposure to QDs can be correlated with the release of Cd^{2+}.

Interaction of QDs with Cell Surface Receptors and Routes of Internalization. MPA-QDs quickly interacted with cell membranes and were internalized in minutes (Supporting Information, movie 1), whereas the uptake of THIO-QDs by macrophages was slower, which we attribute to the propensity of THIO-QDs to form large aggregates in serum-free media. We were able to colocalize MPA-QDs and lysosomes, and their trafficking throughout the cell was recorded in real time (Figure 4and Supporting Information, movie 2). Clift et al.[47] reported that macrophages internalized QDs within minutes, and Zhang et al.[23] demonstrated that upon internalization, the QDs are both vesicle bound and localize to lysosomes in keratinocytes. Previously, small, thioglycolic acid capped CdTe QDs (2.1 nm) were found to be internalized by macrophages within 10 min and localized to the nucleus and perinuclear space, while larger CdTe QDs (3.4 nm) localized within cytoplasmic compartments after 30 min.[24] Murine macrophages treated with carboxylated QDs were found to internalize QDs within 30 min, while cells treated with NH2-PEG coated QDs internalized QDs more slowly. In the current study, THIO-QDs aggregated in media and were found to be much larger in size compared to MPA-QDs and were internalized at a slower rate. However, this aggregation caused interference when performing colocalization imaging studies; thus, we were unable to definitively conclude that THIO-QDs are sequestered in lysosomes.

Both QDs suspended in RPMI + FBS primarily enter macrophages via clathrin coated pits since incubation with a clathrin inhibitor significantly decreased QD uptake (Figure 3). Thus, particles of very different sizes and similar negative charges are being internalized by similar mechanisms. Work investigating nonspecific QD uptake in tumor cell lines revealed that carboxylated QDs were internalized via receptor-mediated endocytosis and clathrin coated pits.[48] In other studies, negative QDs were found to enter keratinocytes via lipid rafts, and little interaction with clathrin was observed.[23] These differences may be attributed to the fact that macrophages have a large number of clathrin coated pits, and other cells, such as fibroblasts and endothelial cells, have been found to have a greater number of caveolae.[49]

The presence of FBS in media appeared to diminish the association of both MPA-QDs and THIO-QDs with macrophages (Table 3). This indicates that serum proteins compete with QDs for interactions with the cell surface; alternatively, serum constituents may coat QDs, reducing their interactions with the cell surface. Table 1 shows the changes in size and charge upon the addition of Poly-I (100 μg/mL) to MPA-QDs. In all three media, there is a slight reduction in size, and the particles remain negatively charged. We are proposing that there is minimal interaction between Poly-I and MPA-QDs.

Thus, the decrease in cellular fluorescence in the presence of Poly-I, indicates that MPA-QDs associate with scavenger receptors (Figure 7). However, there are clearly other receptors that participate in MPA-QD binding since cell fluorescence was reduced and not eliminated altogether in the presence of this scavenger−receptor ligand. One recent study supporting this observation found that citrate stabilized negatively charged gold nanoparticles (less than 100 nm) were internalized using scavenger−receptor mediated phagocytosis.[50]

In the case of RPMI (Figure 7), we conclude that surface charge is playing a major role in QD and scavenger−receptor association. While both MPA-QDs and THIO-QDs were less than 62 nm in size when suspended in RPMI, they had very different surface charges (−34 mV for MPA-QDs and +15 for THIO-QDs). Thus, the only case where the THIO-QDs retain their positive charge and small size (comparable to MPA-QDs) is in RPMI media. A direct comparison can therefore be made as to the influence of charge on nanoparticle uptake in RPMI. It is evident from Table 3 that the uptake of THIO-QDs is lower than that of MPA-QDs in RPMI (e.g., at 62.5 nM concentration, percent of fluorescent cells for MPA-QD and THIO-QD are 92% and 67%, respectively). We propose that the positively charged QDs do not use the scavenger receptor pathway to enter the cell but perhaps interact with a receptor that is expressed at lower levels on the cell surface, whereas negatively charged QD use this pathway, explaining the higher

uptake. In the presence of Poly-I, the MPA-QD remain small (17 nm) and negatively charged, and Poly-I blocks the scavenger receptor mediated uptake of the negative particles. Several groups have investigated the role of scavenger receptors and their affinity to negatively charged molecules.[51−54] The scavenger receptor MARCO (macrophage receptor with collagenous structure) was found to have a positively charged basic cluster containing several arginine residues.[55] In the case of THIO-QD, the Poly-I interacts with the QD itself, and large negatively charged particles are formed, and their entry into the cell takes place by other pathways. Large, negatively charged particles are also noted with THIO-QDs in RPMI + FBS, both in the absence and presence of Poly-I. In the case of X-VIVO, large neutral aggregates are observed for THIO-QDs in the absence and presence of Poly-I. These large, negative or neutral particles are not involved with scavenger receptors in their uptake.

Both THIO-QDs and MPA-QDs induced apoptosis at large concentrations. Interaction of silica and scavenger receptors has been shown to induce apoptosis in Chinese hamster ovary cell lines and in MH-S cells, the cell type used in this study.[56,57] Thus, the apoptotic response caused by MPA-QDs can be attributed to the engagement of MPA-QDs with scavenger receptors. THIO-QDs form large clusters (140 and 1200 nm), which suggests that particle aggregate size could also be an important factor modulating interactions with these receptors which can trigger apoptosis. Similar observations were made for THIO-QDs suspended in X-VIVO media. While THIO-QDs did not associate with scavenger receptors, they were found to leach greater amounts free Cd^{2+} which can induce apoptosis as well.

In summary, this study has directly compared differences between MPA-QD and THIO-QD toxicity, and cellular internalization and cell surface associations in macrophages. We observed that biological culture conditions can modulate QD charge and size, thus having a direct impact on cellular responses. These findings have important implications for the use of nanomaterials in biological applications.

■ ASSOCIATED CONTENT

Supporting Information

Colocalization analysis of raw data image stacks; dynamic light scattering and zeta potential for QDs in all media; necrosis of macrophages after 24, 48 or 72 h of exposure; apoptosis of macrophages after 24 h of exposure to 500 nM of MPA-QDs or THIO-QDs; movie of cell−MPA-QD interactions in real time; and movie of MPA-QD/lysosome compartmentalization. This material is available free of charge via the Internet at http://pubs.acs.org.

■ AUTHOR INFORMATION

Corresponding Author

*(P.K.D.) Tel: 614-292-4532. E-mail: dutta@chemistry.ohio-state.edu. (W.J.W.) Tel: 614-292-7772. E-mail: james.waldman@osumc.edu.

Funding

This work was performed under NIOSH Grant R01 OH009141 and USDA/NIFA (2011-67021-30360).

■ ACKNOWLEDGMENTS

We are grateful to Dr. Rashi Iyer at Los Alamos National Laboratory for her thoughtful discussion and suggestions for improving this manuscript. We also thank the Ohio State University Campus Microscopy and Imaging Facility for use of the live cell confocal imaging system.

■ ABBREVIATIONS

QDs, quantum dots; ROS, reactive oxygen species; TNF-α, tumor necrosis factor-alpha; IL-1β, Interleukin 1-beta; MPA, mercaptopropionic acid; MPA-QDs, mercaptopropionic acid capped QDs; THIO-QDs, thiocholine capped QDs; ICP-MS, inductively coupled plasma mass spectroscopy; RPMI, Roswell Park Memorial Institute media; FBS, fetal bovine serum; LDH, lactate dehydrogenase; Poly-I, Poly-inosinic acid

■ REFERENCES

(1) Chen, L., Sheng, Z., Zhang, A., Guo, X., Li, J., Han, H., and Jin, M. (2010) Quantum-dots-based fluoroimmunoassay for the rapid and sensitive detection of avian influenza virus subtype H5N1. *Luminescence 25*, 419−423.

(2) Fu, X., Huang, K., and Liu, S. (2009) A robust and fast bacteria counting method using CdSe/ZnS core/shell quantum dots as labels. *J. Microbiol. Methods 79*, 367−370.

(3) Tripp, R. A., Alvarez, R., Anderson, B., Jones, L., Weeks, C., and Chen, W. (2007) Bioconjugated nanoparticle detection of respiratory syncytial virus infection. *Int. J. Nanomed. 2*, 117−124.

(4) Zeng, Q., Zhang, Y., Song, K., Kong, X., Aalders, M. C., and Zhang, H. (2009) Enhancement of sensitivity and specificity of the fluoroimmunoassay of Hepatitis B virus surface antigen through "flexible" coupling between quantum dots and antibody. *Talanta 80*, 307−312.

(5) Weng, K. C., Noble, C. O., Papahadjopoulos-Sternberg, B., Chen, F. F., Drummond, D. C., Kirpotin, D. B., Wang, D., Hom, Y. K., Hann, B., and Park, J. W. (2008) Targeted tumor cell internalization and imaging of multifunctional quantum dot-conjugated immunoliposomes in vitro and in vivo. *Nano Lett. 8*, 2851−2857.

(6) Wu, X., Liu, H., Liu, J., Haley, K. N., Treadway, J. A., Larson, J. P., Ge, N., Peale, F., and Bruchez, M. P. (2003) Immunofluorescent labeling of cancer marker Her2 and other cellular targets with semiconductor quantum dots. *Nat. Biotechnol. 21*, 41−46.

(7) Yang, L., Mao, H., Wang, Y. A., Cao, Z., Peng, X., Wang, X., Duan, H., Ni, C., Yuan, Q., Adams, G., Smith, M. Q., Wood, W. C., Gao, X., and Nie, S. (2009) Single chain epidermal growth factor receptor antibody conjugated nanoparticles for in vivo tumor targeting and imaging. *Small 5*, 235−243.

(8) Bagalkot, V., Zhang, L., Levy-Nissenbaum, E., Jon, S., Kantoff, P. W., Langer, R., and Farokhzad, O. C. (2007) Quantum dot-aptamer conjugates for synchronous cancer imaging, therapy, and sensing of drug delivery based on bi-fluorescence resonance energy transfer. *Nano Lett. 7*, 3065−3070.

(9) Holden, C. A., Yuan, Q., Yeudall, W. A., Lebman, D. A., and Yang, H. (2010) Surface engineering of macrophages with nanoparticles to generate a cell-nanoparticle hybrid vehicle for hypoxia-targeted drug delivery. *Int. J. Nanomed. 5*, 25−36.

(10) Liu, Y., Steiniger, S. C., Kim, Y., Kaufmann, G. F., Felding-Habermann, B., and Janda, K. D. (2007) Mechanistic studies of a peptidic GRP78 ligand for cancer cell-specific drug delivery. *Mol. Pharmaceutics 4*, 435−447.

(11) Courty, S., Luccardini, C., Bellaiche, Y., Cappello, G., and Dahan, M. (2006) Tracking individual kinesin motors in living cells using single quantum-dot imaging. *Nano Lett. 6*, 1491−1495.

(12) Dahan, M., Lévi, S., Luccardini, C., Rostaing, P., Riveau, B., and Triller, A. (2003) Diffusion dynamics of glycine receptors revealed by single-quantum dot tracking. *Science 302*, 442−445.

(13) Srinivasan, C., Lee, J., Papadimitrakopoulos, F., Silbart, L. K., Zhao, M., and Burgess, D. J. (2006) Labeling and intracellular tracking of functionally active plasmid DNA with semiconductor quantum dots. *Mol. Ther. 14*, 192−201.

(14) Tada, H., Higuchi, H., Wanatabe, T. M., and Ohuchi, N. (2007) In vivo real-time tracking of single quantum dots conjugated with monoclonal anti-HER2 antibody in tumors of mice. *Cancer Res. 67*, 1138−1144.
(15) Courty, S., Bouzigues, C., Luccardini, C., Ehrensperger, M. V., Bonneau, S., and Dahan, M. (2006) Tracking individual proteins in living cells using single quantum dot imaging. *Methods Enzymol. 414*, 211−228.
(16) Joo, K. I., Lei, Y., Lee, C. L., Lo, J., Xie, J., Hamm-Alvarez, S. F., and Wang, P. (2008) Site-specific labeling of enveloped viruses with quantum dots for single virus tracking. *ACS Nano 2*, 1553.
(17) Jaiswal, J. K., Mattoussi, H., Mauro, J. M., and Simon, S. M. (2003) Long-term multiple color imaging of live cells using quantum dot bioconjugates. *Nat. Biotechnol. 21*, 47−51.
(18) Lidke, D. S., Nagy, P., Heintzmann, R., Arndt-Jovin, D. J., Post, J. N., Grecco, H. E., Jares-Erijman, E. A., and Jovin, T. M. (2004) Quantum dot ligands provide new insights into erbB/HER receptor-mediated signal transduction. *Nat. Biotechnol. 22*, 198−203.
(19) Shiohara, A., Hoshino, A., Hanaki, K., Suzuki, K., and Yamamoto, K. (2004) On the cyto-toxicity caused by quantum dots. *Microbiol. Immunol. 48*, 669−675.
(20) Lovrić, J., Bazzi, H. S., Cuie, Y., Fortin, G. R., Winnik, F. M., and Maysinger, D. (2005) Differences in subcellular distribution and toxicity of green and red emitting CdTe quantum dots. *J. Mol. Med. 83*, 377.
(21) Lovrić, J., Cho, S. J., Winnik, F. M., and Maysinger, D. (2005) Unmodified cadmium telluride quantum dots induce reactive oxygen species formation leading to multiple organelle damage and cell death. *Chem. Biol. 12*, 1227.
(22) Tang, M., Xing, T., Zeng, J., Wang, H., Li, C., Yin, S., Yan, D., Deng, H., Liu, J., Wang, M., Chen, J., and Ruan, D. Y. (2008) Unmodified CdSe quantum dots induce elevation of cytoplasmic calcium levels and impairment of functional properties of sodium channels in rat primary cultured hippocampal neurons. *Environ. Health Perspect. 116*, 915−922.
(23) Zhang, L. W., and Monteiro-Riviere, N. A. (2009) Mechanisms of quantum dot nanoparticle cellular uptake. *Toxicol. Sci. 110*, 138.
(24) Nabiev, I., Mitchell, S., Davies, A., Williams, Y., Kelleher, D., Moore, R., Gun'ko, Y. K., Byrne, S., Rakovich, Y. P., Donegan, J. F., Sukhanova, A., Conroy, J., Cottell, D., Gaponik, N., Rogach, A., and Volkov, Y. (2007) Nonfunctionalized nanocrystals can exploit a cell's active transport machinery delivering them to specific nuclear and cytoplasmic compartments. *Nano Lett. 7*, 3452.
(25) Williams, Y., Sukhanova, A., Nowostawska, M. l. G., Davies, A. M., Mitchell, S., Oleinikov, V., Gun'ko, Y., Nabiev, I., Kelleher, D., and Volkov, Y. (2009) Probing cell-type-specific intracellular nanoscale barriers using size-tuned quantum dots. *Small 5*, 2581−2588.
(26) Schumacher, W., Nagy, A., Waldman, W. J., and Dutta, P. K. (2009) Direct synthesis of aqueous CdSe/ZnS-based quantum dots using microwave irradiation. *J. Phys. Chem. C 113*, 12132−12139.
(27) Provencher, S. W. (1982) A constrained regularization method for inverting data represented by linear algebraic or integral equations. *Comput. Phys. Commun. 27*, 213−227.
(28) Li, H. H. (1984) Refractive index of ZnS, ZnSe, and ZnTe and its wavelength and temperature derivatives. *J. Phys. Chem. Ref. Data 13*, 104−148.
(29) Fernando, Q., and Freiser, H. (1958) Chelating properties of β-mercaptopropionic acid. *J. Am. Chem. Soc. 80*, 4928−4931.
(30) Zhang, Y., Chen, Y., Westerhoff, P., and Crittenden, J. C. (2008) Stability and removal of water soluble CdTe quantum dots in water. *Environ. Sci. Technol. 42*, 321−325.
(31) Lundqvist, M., Stigler, J., Elia, G., Lynch, I., Cedervall, T., and Dawson, K. A. (2008) Nanoparticle size and surface properties determine the protein corona with possible implications for biological impacts. *Proc. Natl. Acad. Sci. U.S.A. 105*, 14265−14270.
(32) Maiorano, G., Sabella, S., Sorce, B., Brunetti, V., Malvindi, M. A., Cingolani, R., and Pompa, P. P. (2010) Effects of cell culture media on the dynamic formation of protein/nanoparticle complexes and influence on the cellular response. *ACS Nano 4*, 7481−7491.
(33) Warnement, M. R., Tomlinson, I. D., Chang, J. C., Schreuder, M. A., Luckabaugh, C. M., and Rosenthal, S. J. (2008) Controlling the reactivity of ampiphilic quantum dots in biological assays through hydrophobic assembly of custom PEG derivatives. *Bioconjugate Chem. 19*, 1404−1413.
(34) Hanaki, K., Momo, A., Oku, T., Komoto, A., Maenosono, S., Yamaguchi, Y., and Yamamoto, K. (2003) Semiconductor quantum dot/albumin complex is a long-life and highly photostable endosome marker. *Biochem. Biophys. Res. Commun. 302*, 496−501.
(35) Doorley, G. W., and Payne, C. K. (2011) Cellular binding of nanoparticles in the presence of serum proteins. *Chem. Commun. 47*, 466−468.
(36) Chan, W. H., Shiao, N. H., and Lu, P. Z. (2006) CdSe quantum dots induce apoptosis in human neuroblastoma cells via mitochondrial-dependent pathways and inhibition of survival signals. *Toxicol. Lett. 167*, 191−200.
(37) Su, Y., He, Y., Lu, H., Sai, L., Li, Q., Li, W., Wang, L., Shen, P., Huang, Q., and Fan, C. (2009) The cytotoxicity of cadmium based, aqueous phase-synthesized, quantum dots and its modulation by surface coating. *Biomaterials 30*, 19−25.
(38) Li, K. G., Chen, J. T., Bai, S. S., Wen, X., Song, S. Y., Yu, Q., Li, J., and Wang, Y. Q. (2009) Intracellular oxidative stress and cadmium ions release induce cytotoxicity of unmodified cadmium sulfide quantum dots. *Toxicol. in Vitro 23*, 1007−1013.
(39) Han, S. G., Castranova, V., and Vallyathan, V. (2007) Comparative cytotoxicity of cadmium and mercury in a human bronchial epithelial cell line (BEAS-2B) and its role in oxidative stress and induction of heat shock protein 70. *J. Toxicol. Environ. Health, Part A 70*, 852−860.
(40) Derfus, A. M., Chan, W. C. W., and Bhatia, S. N. (2003) Probing the cytotoxicity of semiconductor quantum dots. *Nano Lett. 4*, 11−18.
(41) Hoshino, A., Fujioka, K., Oku, T., Suga, M., Sasaki, Y. F., Ohta, T., Yasuhara, M., Suzuki, K., and Yamamoto, K. (2004) Physicochemical properties and cellular toxicity of nanocrystal quantum dots depend on their surface modification. *Nano Lett. 4*, 2163−2169.
(42) Hoshino, A., Hanada, S., and Yamamoto, K. (2011) Toxicity of nanocrystal quantum dots: the relevance of surface modifications. *Arch. Toxicol. 85*, 707−720.
(43) Xu, J., Xu, F., and Lin, Y. (2011) Cigarette smoke synergizes lipopolysaccharide-induced interieukin-1{beta} and tumor necrosis factor-alpha; secretion from macrophages via substance P-mediated nuclear factor-{kappa}B activation. *Am. J. Respir. Cell Mol. Biol. 44*, 302−308.
(44) Ghiazza, M., Polimeni, M., Fenoglio, I., Gazzano, E., Ghigo, D., and Fubini, B. (2010) Does vitreous silica contradict the toxicity of the crystalline silica paradigm? *Chem. Res. Toxicol. 23*, 620−629.
(45) Lee, H. M., Shin, D. M., Song, H. M., Yuk, J. M., Lee, Z. W., Lee, S. H., Hwang, S. M., Kim, J. M., Lee, C. S., and Jo, E. K. (2009) Nanoparticles up-regulate tumor necrosis factor-alpha and CXCL8 via reactive oxygen species and mitogen-activated protein kinase activation. *Toxicol. Appl. Pharmacol. 238*, 160.
(46) Hyun, J. S., Satsu, H., and Shimizu, M. (2007) Cadmium induces interleukin-8 production via NF-kappaB activation in the human intestinal epithelial cell, Caco-2. *Cytokine 37*, 26−34.
(47) Clift, M. J., Rothen-Rutishauser, B., Brown, D. M., Duffin, R., Donaldson, K., Proudfoot, L., Guy, K., and Stone, V. (2008) The impact of different nanoparticle surface chemistry and size on uptake and toxicity in a murine macrophage cell line. *Toxicol. Appl. Pharmacol. 232*, 418.
(48) Kelf, T. A., Sreenivasan, V. K., Sun, J., Kim, E. J., Goldys, E. M., and Zvyagin, A. V. (2010) Non-specific cellular uptake of surface-functionalized quantum dots. *Nanotechnology 21*, 285105.
(49) Parton, R. G., and Simons, K. (2007) The multiple faces of caveolae. *Nat. Rev. Mol. Cell Biol. 8*, 185−194.
(50) França, A., Aggarwal, P., Barsov, E. V., Kozlov, S. V., Dobrovolskaia, M. A., and González-Fernández, A. (2011) Macrophage scavenger receptor A mediates the uptake of gold colloids by macrophages in vitro. *Nanomedicine 6*, 1175−1188.

(51) Geiser, M., Casaulta, M., Kupferschmid, B., Schulz, H., Semmler-Behnke, M., and Kreyling, W. (2007) The role of macrophages in the clearance of inhaled ultrafine titanium dioxide particles. *Am. J. Respir. Cell Mol. Biol.*, 2007−0138OC.
(52) Hamilton, R. F. Jr., Thakur, S. A., Mayfair, J. K., and Holian, A. (2006) MARCO mediates silica uptake and toxicity in alveolar macrophages from C57BL/6 mice. *J. Biol. Chem. 281*, 34218−34226.
(53) Kanno, S., Furuyama, A., and Hirano, S. (2007) A murine scavenger receptor MARCO recognizes polystyrene nanoparticles. *Toxicol. Sci. 97*, 398−406.
(54) Thakur, S. A., Hamilton, R. Jr., Pikkarainen, T., and Holian, A. (2009) Differential binding of inorganic particles to MARCO. *Toxicol. Sci. 107*, 238−246.
(55) Ojala, J. R., Pikkarainen, T., Tuuttila, A., Sandalova, T., and Tryggvason, K. (2007) Crystal structure of the cysteine-rich domain of scavenger receptor MARCO reveals the presence of a basic and an acidic cluster that both contribute to ligand recognition. *J. Biol. Chem. 282*, 16654.
(56) Hamilton, R. F., de Villiers, W. J. S., and Holian, A. (2000) Class A type II scavenger receptor mediates silica-induced apoptosis in Chinese hamster ovary cell line. *Toxicol. Appl. Pharmacol. 162*, 100−106.
(57) Chao, S. K., Hamilton, R. F., Pfau, J. C., and Holian, A. (2001) Cell surface regulation of silica-induced apoptosis by the SR-A scavenger receptor in a murine lung macrophage cell line (MH-S). *Toxicol. Appl. Pharmacol. 174*, 10−16.